Acoustic characterization of the compressor stage of an automotive turbocharger

I. JAIMES[a,b], A. MILLOT [b], J. CHARLEY[a]

a. Laboratoire de mécanique de Lille (LML) – CNRS : UMR8107, Arts et Métiers ParisTech-Bâtiment M6, Bvd. Paul Langevin 59655 VILLENEUVE D'ASCQ CEDEX, France. Emails : jacques.charley@ensam.eu, isaac.jaimes@ensam.eu

b. CRITTM2A SAS - Rue Christophe Colomb - Parc de la Porte Nord 62700 BRUAY LA BUISSIERE, France. Email : amillot@crittm2a.com, ijaimes@crittm2a.com

…

Abstract:

Turbochargers are a key component of internal combustion engines in the automotive industry. They contribute to the downsizing trend and allow constructors to respect more and more severe emissions norms. However, the turbocharger behaves as an acoustic source in the air intake system, and has an influence in the acoustic waves travelling in it. The passive and active acoustic characteristics of the turbocharger can be used as a starting point for the design and development of acoustic devices in the air intake system, or as an input of acoustic 1D simulations of engine intake lines. In this paper both the active and passive acoustic behaviours of a compressor stage of two different automotive turbochargers were studied. The active acoustic effect of the compressor was studied by its characterization as an acoustic source. This is performed experimentally by the computation of the acoustic intensity at the inlet and outlet of the compressor. This intensity was obtained by performing plane wave decomposition with the beamforming method over all the working points of the compressor map. In this way the acoustic power delivered by the compressor on the air intake system is measured. The passive acoustic effect is studied by the measurement of the acoustic Transmission Loss (TL) of the compressor through the calculation of its scattering matrix under two port considerations. Using also the beamforming method to decompose the incident and reflected waves at the inlet and outlet of the compressor, the transmission coefficients in both upwards and downwards directions are computed. Experimentally the TL of a static turbocharger was measured and results were extrapolated by a model to obtain the TL of the compressor over different working points of the compressor map. Numerically, 3D acoustic simulations were performed in order to compare to the model results. Numerical and experimental results were compared, and a predictive model for TL is proposed. This model will be compared in the future to real TL measurements on a working turbocharger.

Key words: Turbocharger, in-duct acoustics, beamforming, transmission loss

1 Introduction

Downsizing is a common trend in automotive engine development. It is an important technique used by OEMs to respect European and international emissions norms [21]. One way to achieve downsizing efficiently is turbocharging. On the same note, there are as well noise emissions norms [22] that are just as constraining as emissions norms. The combination of these two restrictions (noise and emissions) is why it appears interesting to characterize the turbocharger as an acoustic source in order to develop solutions (such as mufflers) to respect these noise norms. In this paper, focus is on the acoustic characterization of the compressor stage of a turbocharger. First as an acoustic source, and more precisely in the measurement of the acoustic intensity delivered by the turbocharger on the engine compressor inlet and outlet. Secondly, the influence of the turbocharger on an acoustic wave that travels through it, which can be determined by the expression of acoustic characteristic matrices. The most recent research in this topic has been done at KTH's lab CICERO on the characterization of turbocharger acoustics [8-11]. The measurement of acoustic intensity has two main advantages in this case: first, it is a vector quantity, which means it has a magnitude, but also a direction of propagation which helps to differentiate waves travelling upstream and downstream the air intake line. Second, when sound intensity is integrated over a surface, the acoustic power can be obtained. This new quantity can be considered to be constant over the ducts (by neglecting attenuation and considering ducts as not acoustically transparent) and then doesn't depend on the location of the measurement, opposite to pressure measurements.

2 Acoustic characterization methods

2.1 The use of beamforming for plane wave decomposition

To compute the acoustic intensity at the inlet and outlet of the compressor a plane wave decomposition methodology is necessary. One technique for performing this is the well stablished Two Microphone Method (TMM) [7, 13]. However, recent research [2, 3, 12, 20] has shown that the beamforming technique applied in this context can deliver promising results, mostly because it's less sensitive to turbulent airflow noise. Beamforming is used more commonly for acoustic source localization [6] by sweeping several directions of arrival and identifying the maximum amplitude at a given direction which corresponds to the location of the acoustic source. In this application, instead of sweeping several directions of arrival, the microphone array is steered to acquire the pressure of a known source and then quantify it. The name beamforming comes from the "formation of beams", meaning that the sensitivity of an array of sensors can be steered in a specific direction thus forming a beam in that direction. The principle of the technique is to have several sensors separated by a certain known distance. The signals of the sensors are multiplied by some weight factors in order to receive the energy coming from a certain direction of arrival in priority. Therefore, beamforming can be considered as spatial filtering [4]. Pinero et. al have used it on exhaust systems [18, 19] to obtain velocity fluctuations in automotive exhaust systems.

The beamforming method consists in multiplying the pressure measured by each sensor of the array by a weighting factor and adding the results to acquire the pressure of a wave arriving from a known direction of arrival (DoA). The expression of the output of a beamformer with N sensors in the time domain can be expressed by equation (2.1.1). $p_\theta(t)$ is the pressure of a wave arriving from direction θ as shown in Figure 1. $p_n(t)$ is the pressure of each of the n sensors of the array, and $w^*_{n,\theta}$ are the determined weighting factors for each sensor. The main difficulty of beamforming is then to determine the right weighting factors.

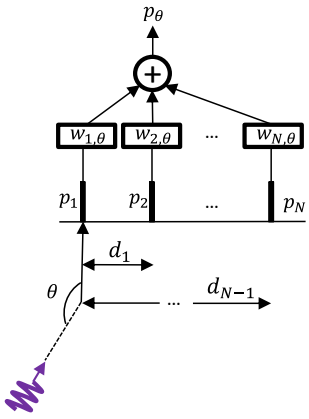

Fig. 1: Beamforming principle

$$p_\theta(t) = \sum_{n=1}^{N} w_{n,\theta}^{*}\, p_n(t) \tag{2.1.1}$$

In this study, the beamformer is limited to three sensors in order to have a compact array of microphones that can potentially be mounted in a working automotive engine. Let us first apply the measurement technique to a monochromatic wave of frequency f propagating in a duct.

$$s(t) = s_0(t)e^{j\omega t} = s_0(t)e^{j2\pi ft} \tag{2.1.2}$$

The study is limited to the plane wave frequency range so the pressure at each of the three sensors can be expressed as a delay of a source plane wave propagating following the direction of the duct:

$$\begin{aligned} p_n(t) &= s_0(t-\tau_n)\, e^{j\omega(t-\tau_{n,\theta})} \\ &= s_0(t)\, e^{j\omega(t-\tau_{n,\theta})} \\ &= s(t)\, e^{-j\omega\tau_{n,\theta}} \end{aligned} \tag{2.1.3}$$

By arbitrarily choosing the first sensor as the origin of phases, $\tau_{n,\theta}$ is the time delay that takes the signal arriving from the direction θ to arrive at sensor n as shown in Figure 2, so for each one of the three sensors:

$$\tau_{1,\theta} = 0,\ \ \tau_{2,\theta} = \frac{d_1 sin(\theta)}{c_0(1+M)},\ \ \tau_{3,\theta} = \frac{d_2 sin(\theta)}{c_0(1+M)} \tag{2.1.4}$$

c_0: speed of sound (m/s).

M: main Mach number of the air flow.

By using equations (2.1.4) in equation (2.1.3), the pressures at the three sensors are then written as:

$$\begin{aligned} p_1(t) &= s(t) \\ p_2(t) &= s(t)\, e^{-j\omega\tau_{2,\theta}} \\ p_3(t) &= s(t)\, e^{-j\omega\tau_{3,\theta}} \end{aligned} \tag{2.1.5}$$

In order to use matrix notation for the sake of simplicity, a vector $\boldsymbol{x}(t)$ containing the pressures of the three sensors is created, as well as a vector $\boldsymbol{a}(\theta)$ (called the steering vector) containing the exponential terms of the time delays as shown in equation (2.1.6):

$$\boldsymbol{x}(t) = \begin{bmatrix} p_1(t) \\ p_2(t) \\ p_3(t) \end{bmatrix} = s(t) \begin{bmatrix} 1 \\ e^{-j\omega\tau_{2,\theta}} \\ e^{-j\omega\tau_{3,\theta}} \end{bmatrix} = s(t)\boldsymbol{a}(\theta) \tag{2.1.6}$$

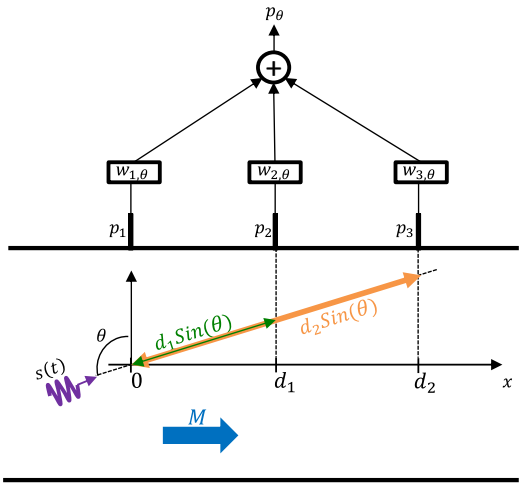

Fig 2: Three sensor beamformer

As we assume plane wave propagation in the duct following the axis of the duct, waves arriving at the sensor array can only have two different directions of arrival: $\theta \in \{+90°, -90°\}$. The two corresponding steering vectors are thus:

$$\boldsymbol{a}(90) = \begin{bmatrix} 1 \\ e^{-j\omega\frac{d_1}{c_0(1+M)}} \\ e^{-j\omega\frac{d_2}{c_0(1+M)}} \end{bmatrix}, \boldsymbol{a}(-90) = \begin{bmatrix} 1 \\ e^{j\omega\frac{d_1}{c_0(1-M)}} \\ e^{j\omega\frac{d_2}{c_0(1-M)}} \end{bmatrix} \tag{2.1.7}$$

Both vectors are used to create the so called steering matrix $\boldsymbol{A}$:

$$\boldsymbol{A} = [\boldsymbol{a}(90) \quad \boldsymbol{a}(-90)] = \begin{bmatrix} 1 & 1 \\ e^{-j\omega\frac{d_1}{c_0(1+M)}} & e^{j\omega\frac{d_1}{c_0(1-M)}} \\ e^{-j\omega\frac{d_2}{c_0(1+M)}} & e^{j\omega\frac{d_2}{c_0(1-M)}} \end{bmatrix} \tag{2.1.8}$$

A vector $\boldsymbol{s}(t)$ containing both arriving pressure waves is expressed as:

$$\boldsymbol{s}(t) = \begin{bmatrix} s_{+90}(t) \\ s_{-90}(t) \end{bmatrix} \tag{2.1.9}$$

So the pressures vector can now be written as a function of the steering vector and the pressures arriving from both directions:

$$\boldsymbol{x}(t) = \boldsymbol{A}\boldsymbol{s}(t) \tag{2.1.10}$$

Finally, the beamformer output is defined as:

$$p_\theta\,(t) = w_\theta^H \boldsymbol{x}(t) \tag{2.1.11}$$

Which is the matrix form of equation (2.1), with the weighting vector:

$$w_\theta = \begin{bmatrix} w_{1,\theta} \\ w_{2,\theta} \\ w_{3,\theta} \end{bmatrix} \tag{2.1.12}$$

The precedent equations can be redefined in the frequency domain through Fourier transform and by using the corrected wave numbers $k^+$and k^-:

$$\boldsymbol{A} = [\boldsymbol{a}(90) \quad \boldsymbol{a}(-90)] = \begin{bmatrix} 1 & 1 \\ e^{-jk^+d_1} & e^{jk^-d_1} \\ e^{-jk^+d_2} & e^{jk^-d_2} \end{bmatrix} \tag{2.1.13}$$

With the corrected wave numbers defined as:

$$k^+ = \frac{k+\alpha(1-j)}{1+M}, \qquad k^- = \frac{k+\alpha(1-j)}{1-M} \tag{2.1.14}$$

Several expressions exist for computing the viscothermal attenuation coefficient α [7]. A study for evaluating the impact of different expressions of α on sound intensity was realized. The differences were negligible and thus the expression used on this paper is the one presented in the following equation:

$$\alpha = \frac{\sqrt{2\nu\omega}}{Dc_0}\left(1 + \frac{\gamma-1}{\sqrt{Pr}}\right) \tag{2.1.15}$$

ν: Kinematic viscosity (m^2/s).
γ: Ratio of specific heats
Pr: Prandtl number

Through Fourier transform equation (2.1.6) becomes:

$$\boldsymbol{X}(f) = \boldsymbol{A}(f)\boldsymbol{S}(f) \tag{2.1.16}$$

And finally, equation (2.1.1) becomes:

$$\boldsymbol{P}_\theta(f) = \boldsymbol{W}_\theta^H \boldsymbol{X}(f) \tag{2.1.17}$$

Different strategies exist for the calculation of the weighting factors of the beamformer. In this paper, the Delay and Sum (DS) beamformer [4] is used as it is relatively easy to compute and no statistic assumptions concerning the data sets are needed. Its goal is to minimize the difference between the array actual response and a desired response. The minimization problem is expressed as:

$$\min_w\{|\boldsymbol{A}^H\boldsymbol{W}_{DS} - \boldsymbol{r}_d|^2\} \tag{2.1.18}$$

And the optimum solution is:

$$\boldsymbol{W}_{DS} = \boldsymbol{A}^{+H}\boldsymbol{r}_d \tag{2.1.19}$$

Where $A^{+H} = (AA^H)^{-1}A$ is the pseudo inverse of A^H and r_d is the matrix containing the desired responses for each direction, forcing amplitude of 1 for the desired direction and nil response for the one:

$$\boldsymbol{r}_d = [r_{df} \quad r_{db}] = \begin{bmatrix}1 & 0\\ 0 & 1\end{bmatrix} \tag{2.1.20}$$

Once the weighting factors are determined, the output of the beamformer in the desired direction can be calculated thanks to equation (2.1.17).

2.2 Active acoustic characterization

Sound intensity is defined as the product of sound pressure p and acoustic velocity $\boldsymbol{u}$:

$$\boldsymbol{I} = p\boldsymbol{u} \tag{2.2.1}$$

Considering plane wave propagation in a duct (below the frequency of the first asymmetric mode in the duct), every pressure wave can be considered as the sum of one incident wave (propagating in the positive direction) and a reflected wave (propagating in the negative direction):

$$p(t,x) = p^+ e^{j(\omega t - k^+ x)} + p^- e^{j(\omega t + k^- x)} \tag{2.2.2}$$

ω: Angular frequency (rad).
k^+: Corrected wave number on the positive direction.
k^-: Corrected wave number on the negative direction.
x: Position over the duct (m).

The linearized Euler equation can be used to link the pressure to the acoustic velocity:

$$j\omega\rho_0 u(x,t) + \frac{\partial p(x,t)}{\partial x} = 0 \tag{2.2.3}$$

ρ_0: Air density (kg/m^3).

Using equation (2.2.3) in equation (2.2.2) we obtain the acoustic velocity as a function of the pressure components:

$$u = \frac{1}{\rho_0 c_0}(p^+ - p^-) \tag{2.2.4}$$

Finally, using Morfey's correction in presence of air mass flow [16], we obtain an expression of acoustic intensity in the duct:

$$I = \frac{1}{\rho_0 c_0}\left(|p^+|^2(1+M^2) - |p^-|^2(1-M^2)\right) \tag{2.2.5}$$

It is now evident why a plane wave decomposition has to be performed for the calculation of the sound intensity in the duct. However, as plane wave propagation is supposed, only plane wave modes should be taken into account. This limits the computation to the frequency range below the first non-plane mode: the so called cut-off frequency. This frequency, as shown by Munjal in [17] is a function of the duct diameter, the speed of sound and the mean air flow velocity and is computed by:

$$f_c = \frac{1.84 c_0 \sqrt{1-M^2}}{\pi D} \tag{2.2.6}$$

D: Duct diameter (m).

This frequency also defines the distance between the pressure sensors for the TMM, as the criterion to avoid significant errors due to sensor's positions is, according to Abom [1,5]:

$$0.1\pi(1-M^2) < kd < 0.8\pi(1-M^2) \tag{2.2.7}$$

This criterion being over restrictive for beamforming, it has been shown [18,19] that by respecting it, errors due to sensor position can be minimized.

2.3 Passive acoustic characterization: Transmission Loss (TL)

The turbocharger compressor, within the air intake system of the vehicle can be considered as an acoustic two port. Its passive acoustic characteristics can then be synthesized by the use of three characteristic matrices: the mobility matrix (or impedance matrix) [15], the transfer matrix [17], and the scattering matrix [14], expressed respectively as:

$$\begin{pmatrix} P_i \\ P_o \end{pmatrix} = \begin{pmatrix} Z_{ii} & Z_{io} \\ Z_{oi} & Z_{oo} \end{pmatrix} \begin{pmatrix} Q_i \\ Q_o \end{pmatrix} \qquad \begin{pmatrix} P_o \\ Q_o \end{pmatrix} = \begin{pmatrix} H_1 & H_2 \\ H_3 & H_4 \end{pmatrix} \begin{pmatrix} P_i \\ Q_i \end{pmatrix} \qquad \begin{pmatrix} P_i^- \\ P_o^+ \end{pmatrix} = \begin{pmatrix} S_{11} & S_{12} \\ S_{21} & S_{22} \end{pmatrix} \begin{pmatrix} P_i^+ \\ P_o^- \end{pmatrix} \tag{2.3.1}$$

The choice of the formalism to use depends on the kind of application that is to be used. Transfer matrices are more adapted to be used when acoustic devices are arranged in a series, obtaining the global transfer matrix as the product of the transfer matrices of each element of the system. Impedance matrix is more adapted to parallel arrangements. In our case, the objective is to compute the Transmission Loss as it constitutes a representative quantity of attenuation performance of an acoustic device. The most adapted formalism for Transmission Loss computation is the scattering matrix formalism, as it can deliver directly transmission coefficients by the terms S_{12} in the downwards direction and S_{21} in the upwards direction. Equation (2.32) illustrates this.

$$TL_S = 10\log\left(\frac{(1+M_i)^2 S_i \rho_o c_o}{(1+M_o)^2 S_o \rho_i c_i} \frac{1}{|S_{21}|^2}\right) \tag{2.3.2}$$

In order to find the four coefficients of the scattering matrix, a two source method can be used, which means that to different excitation cases are needed to have 4 equations and be able to find the 4 terms of the matrix. Beamforming plane wave decomposition is performed as shown in Section 2.1 and after solving the system, the four coefficients of the scattering matrix are expressed by equation (2.3.3).

$$S_{11} = \left(\frac{P_{i_1}^- P_{o_2}^- - P_{i_2}^- P_{o_1}^-}{P_{i_1}^+ P_{o_2}^- - P_{i_2}^+ P_{o_1}^-}\right), \qquad S_{12} = \left(\frac{P_{i_1}^+ P_{i_2}^- - P_{i_1}^- P_{i_2}^+}{P_{i_1}^+ P_{o_2}^- - P_{i_2}^+ P_{o_1}^-}\right),$$
$$S_{21} = \left(\frac{P_{o_2}^- P_{o_1}^+ - P_{o_1}^- P_{o_2}^+}{P_{i_1}^+ P_{o_2}^- - P_{i_2}^+ P_{o_1}^-}\right), \qquad S_{22} = \left(\frac{P_{o_2}^+ P_{i_1}^+ - P_{i_2}^+ P_{o_1}^+}{P_{i_1}^+ P_{o_2}^- - P_{i_2}^+ P_{o_1}^-}\right) \tag{2.3.3}$$

Where sub-indexes i and o mean inlet and outlet, and 1 and 2 refer to each one of the two source cases. Even if the scattering matrix is used in this paper, the same kind of expressions can be derived for the transfer matrix and the mobility matrix for the calculation of Transmission Loss. These expressions are however, more complicated as seen in equations (2.3.4) and (2.3.5). It can be mentioned as well that once one of the three matrices is computed, the two others can be obtained by linear transformations.

$$TL_H = 10\log\left(\frac{1}{4}\,\frac{S_i\rho_o c_o(1+M_i)^2}{S_o\rho_i c_i(1+M_o)^2}\,\left|H_1 + H_2\frac{S_o}{\rho_o c_o} + H_3\frac{\rho_i c_i}{S_i} + \frac{S_o\rho_i c_i}{S_i\rho_o c_o}H_4\right|^2\right) \tag{2.3.4}$$

$$TL_Z = 10\log\left(\frac{1}{4}\,\frac{S_i\rho_o c_o(1+M_i)^2}{S_o\rho_i c_i(1+M_o)^2}\,\left|\frac{Z_{oo}S_o\rho_i c_i}{Z_{oi}S_i\rho_o c_o} - \frac{\rho_i c_i}{Z_{oi}S_i} - \frac{Z_{io}S_o\rho_i c_i}{\rho_o c_o(\rho_i c_i + Z_{ii}S_i)}\right|^2\left|\frac{Z_{ii}S_i+\rho_i c_i}{\rho_i c_i}\right|^2\right) \tag{2.3.5}$$

3 Experimentations

3.1 Active acoustic characterization

In order to characterize the compressor as an acoustic source, sound intensity measurements were performed on a turbocharger gas stand. The acoustic intensity was calculated as explained in section 2.2.The numbers on Figure 3 correspond to: 1: compressor inlet; 2: compressor outlet: 3: turbine inlet and 4: turbine outlet. The pressure sensors are pointed at by small triangles. The corresponding turbocharger used for the tests is mounted on a petrol, 1.1 litre, 4 in line cylinder, 16 valves engine.

Looking at Figure 3, the expert eye on plane wave decomposition might point out something. Typically, to ensure the fact that plane waves are propagating, it is advised that the distance between the source and the decomposition zone should be at least several diameters of length (between 4 and 10 diameters). This wasn't the case in this paper. The reason for this is that compact measurement tubes are necessary if needed to be mounted on a working engine.

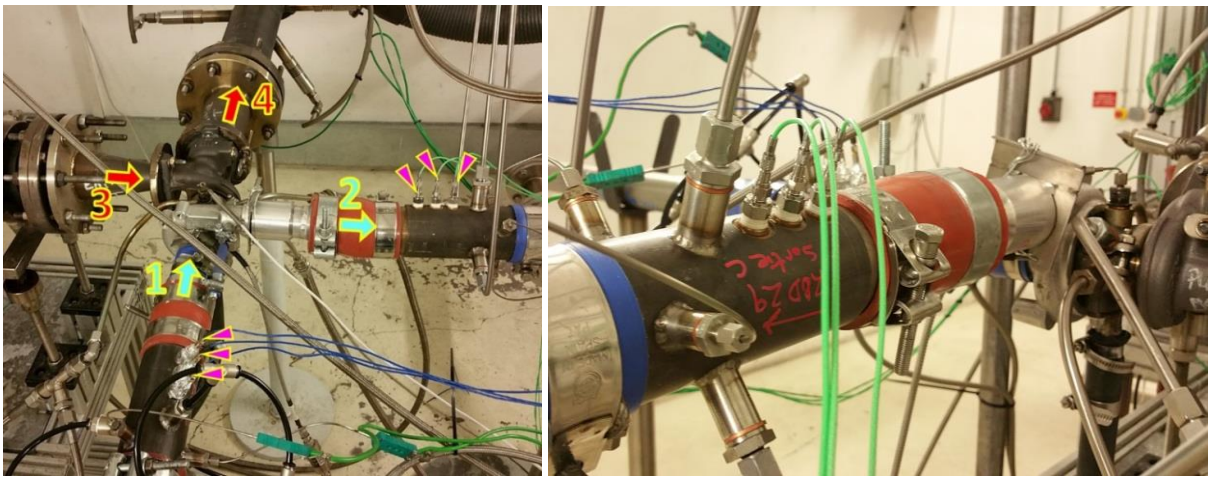

Fig. 3: Turbocharger gas stand test rig.

In turbocharger testing, the more important result is often the full compressor map, which is a plot of the compression ratio (the ratio of the outlet pressure divided by the inlet pressure) versus the air mass flow that passes through the compressor. An exemple of a compressor map is shown in Figure 4. The

limit at the left of the map is known as the surge line. In this region of the map, the pressure ratio is too high corresponding to the air mass flow and thus surge and stall instabilities may appear. The right limit of the map corresponds to the choke line, and it corresponds to the limit of efficiency of the compressor, defined usually between 60% and 50%. The dotted lines correspond to the isospeed lines, where both pressure ratio and mass flow change, but the rotational speed of the compressor remains constant. The solid concentric lines correspond to isoefficiency lines, the center of all of them being the optimal working point of the turbocharger. This kind of maps are used first of all to characterize the performance of the turbocharger, and also to perform turbocharger matching, which means linking the right turbocharger to a certain engine in order to obtain the desired performance.

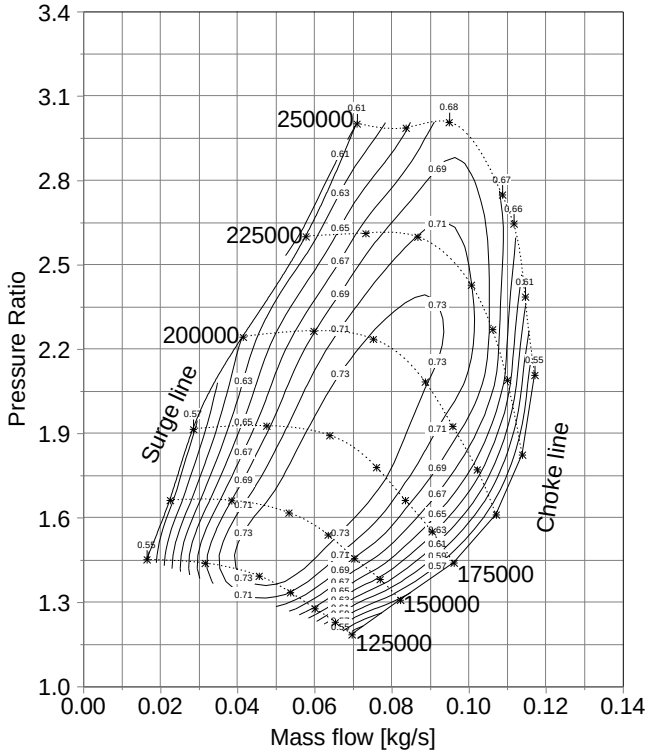

Fig.4: Typical full compressor map.

A full compressor map was performed and acoustic power was computed at each working point. To do so, the total-to-total compression ratio had to be computed, as well as the corrected mass flow. An important point is that mass flow had to be corrected according to temperature, but not corrected according to rotational speed. This is because acoustic phenomena are directly related to rotational speed and the frequencies correspond to the real measured rotational speed.

Figure 5 shows the global sum level of sound Intensity between 400Hz and 4000Hz over each working point and extrapolation between points is done. First it can be noted that the inlet maximum level is almost the same than the outlet minimum level. Globally, the higher is the rotational speed, the higher is the intensity level. Also, in both maps the closer the working point gets to the surge line, the higher is the intensity level. Globally, the higher the rotational speed, the higher the intensity level. The presented maps correspond to a configuration where anechoic terminations were mounted at each end of the compressor branches, but several configurations were tested. Particularly the points close to the surge line.

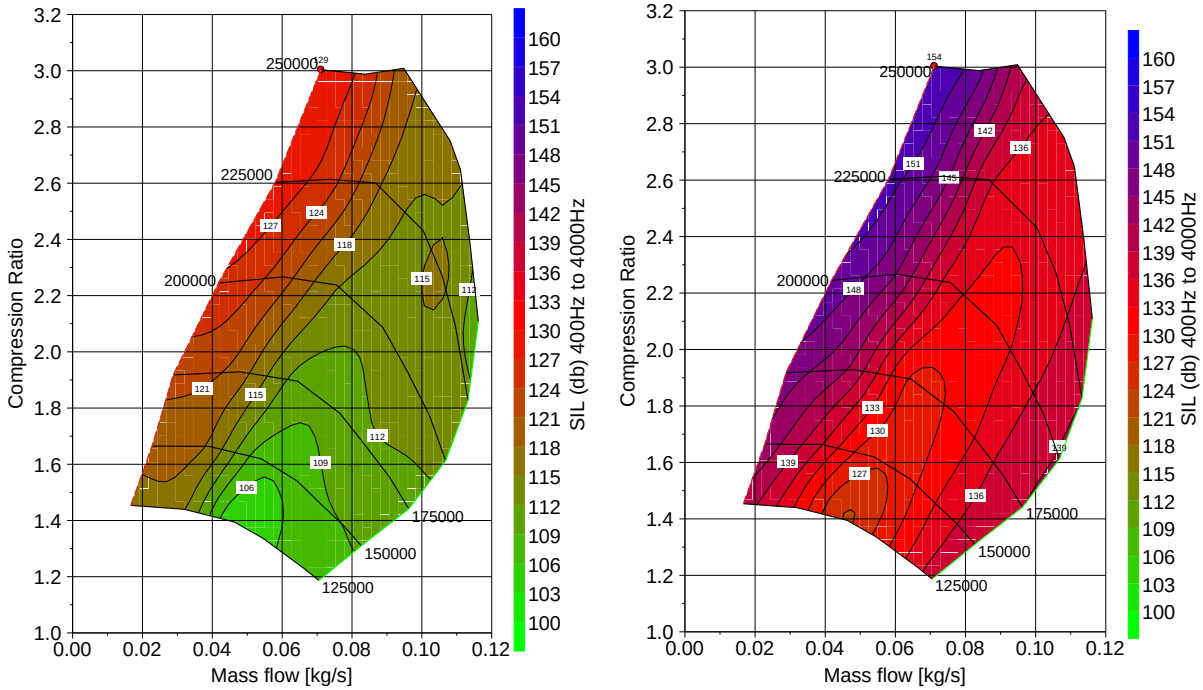

(a) Inlet (b) Outlet

Fig.5: Turbocharger Intensity Level Maps.

3.2 Passive acoustic characterization

In order to characterize the turbocharger as a passive device, both simulations and measurements were performed. To realize FEA on the turbocharger geometry, reverse engineering techniques were used to obtain the CAD of the compressor. The wheel was measured thanks to a 3D measuring machine, which delivers a set of points that can then be converted in a 3D geometry. To construct the volute, an estimation of the geometry was done and modelled in 3D. An assembly of both components was finally used in 3D FE simulations performed with the commercial software VAOne.

The modelled domain was the compressor and both inlet and outlet measurement pipes. The domain had 2749960 acoustic elements and 479871 nodes. The acoustic excitation is created thanks to a steel plate vibrating only on its first mode (piston mode) between 20Hz and 5000Hz. The anechoic termination is performed by using an impedance isolator at the other end. First the acoustic modes of the cavity are computed and then its response to the acoustic excitation is obtained. In figure 6 a global view of the two source cases can be seen. In Figure 7, several detail views of the model can be seen.

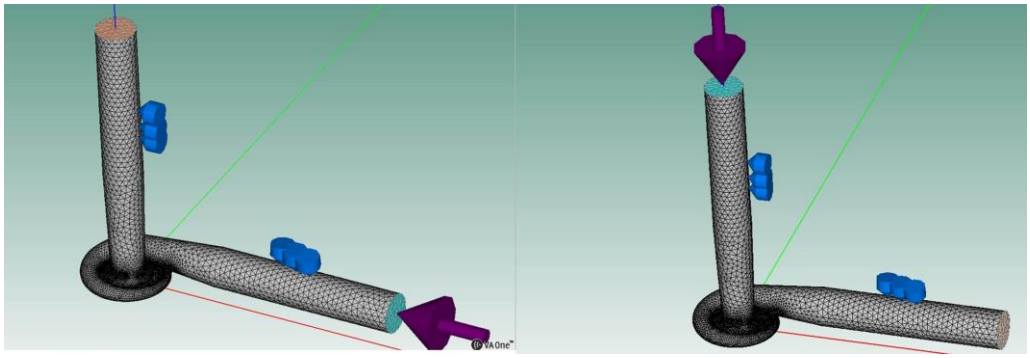

Fig. 6: Global view of the FE simulations

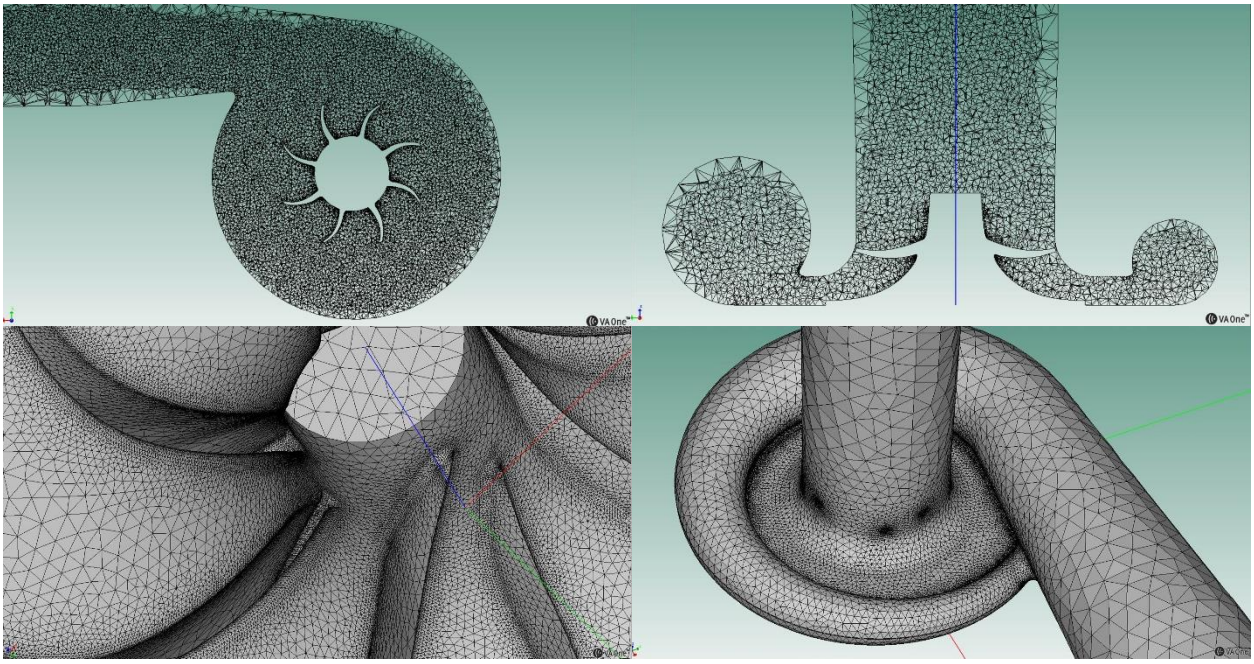

Fig. 7: Detail view of the FE simulations

The modelled acoustic termination was characterized and Figure 8 (b) shows the acoustic impedance that was imposed to the termination. Figure 8 (a) shows the resulting reflexion coefficient.

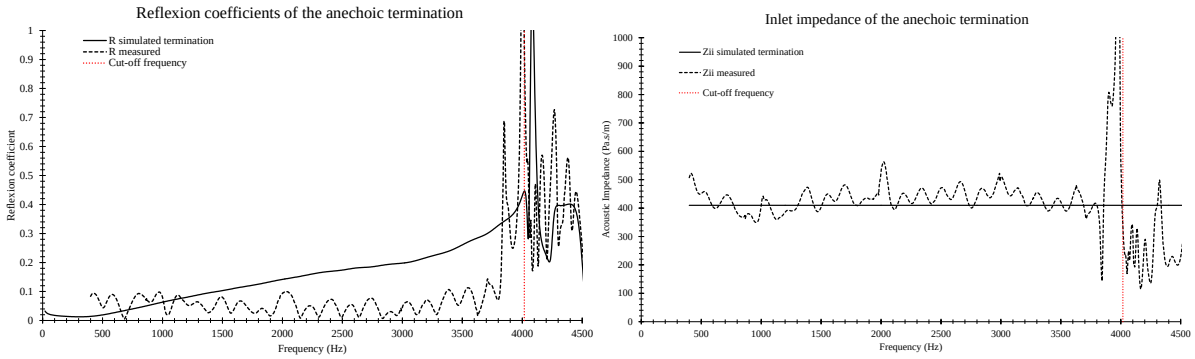

(a) (b)

Fig. 8: Passive acoustic characteristics of the anechoic terminations

In parallel of the simulations, acoustic measurements were performed as shown in Figure 8. An acoustic source was used to excite the turbocharger between 400 Hz and 5000 Hz. A swept sine signal was used to maximize the signal to noise ratio. An anechoic termination was used as well. Its measured inlet impedance and reflexion coefficient were obtained by solving equations (2.3.1) for the termination. The results can be seen in Figures 8 (a) and 8 (b). It can be noticed that the reflexion coefficient of the simulated termination gets higher with frequency. Concerning the impedance, a relatively good correlation is found around the value of 415 Pa.s/m, which corresponds to the characteristic impedance of ambient air. The three characteristic matrices were solved for the turbocharger. The inlet and outlet impedances are shown in Figure 10, compared to the simulated results. A good correlation is shown up to 2000Hz in the curves.

Fig. 9: Test rig for passive acoustic characterization of a static turbocharger

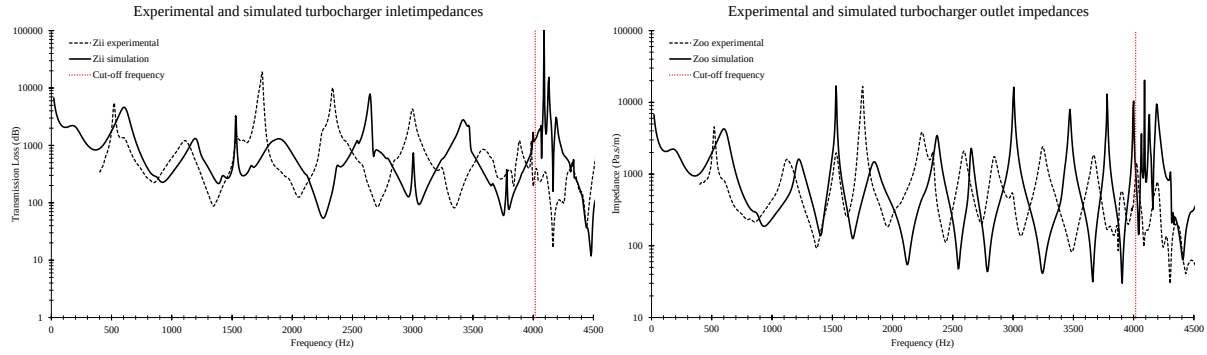

(a) (b)

Fig. 10: Experimental and simulated impedances of the turbocharger

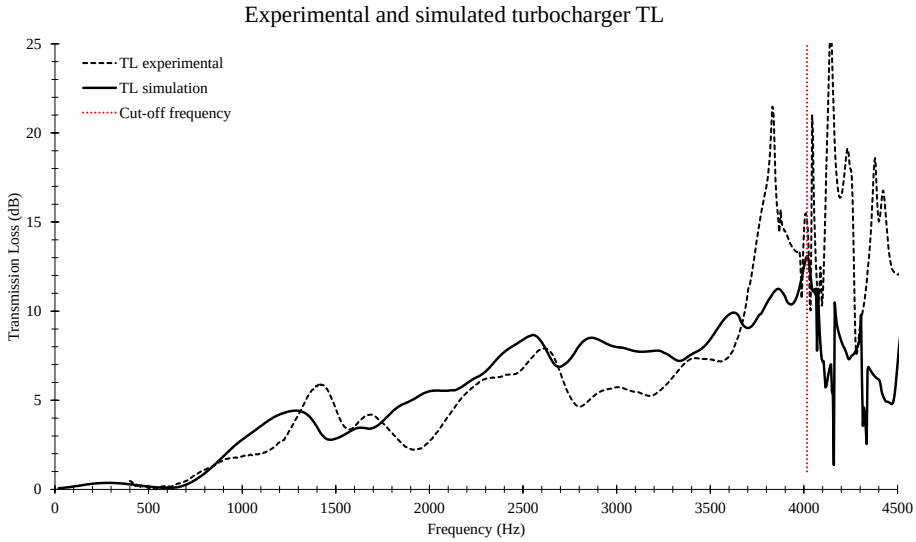

Fig. 11: Experimental and simulated TL of the turbocharger

The final TL results are shown in Figure 11. A good global correlation between tests and simulations is found up to the cut off frequency. The frequency difference might be explained by the volute geometry being an approximation of the actual geometry.

3.2 Transmission Loss Model

Once the TL of the static turbocharger was measured, a model was derived to correct the static TL with the conditions of different working points of the turbocharger. These working points are shown in the compressor map Figure 12. The correcting model intervenes at the final step of the computation of the TL shown in equation (2.3.2), by changing the Mach numbers, speed of sound and air density according

to the different working points. The transfer coefficient $S_{21}$is however kept the same that in the static case, as it is the result of the beamforming decomposition, and the conditions of the decomposition cannot be changed. It is likely however that the transmission coefficient of a rotating turbocharger is different than that of a static one.

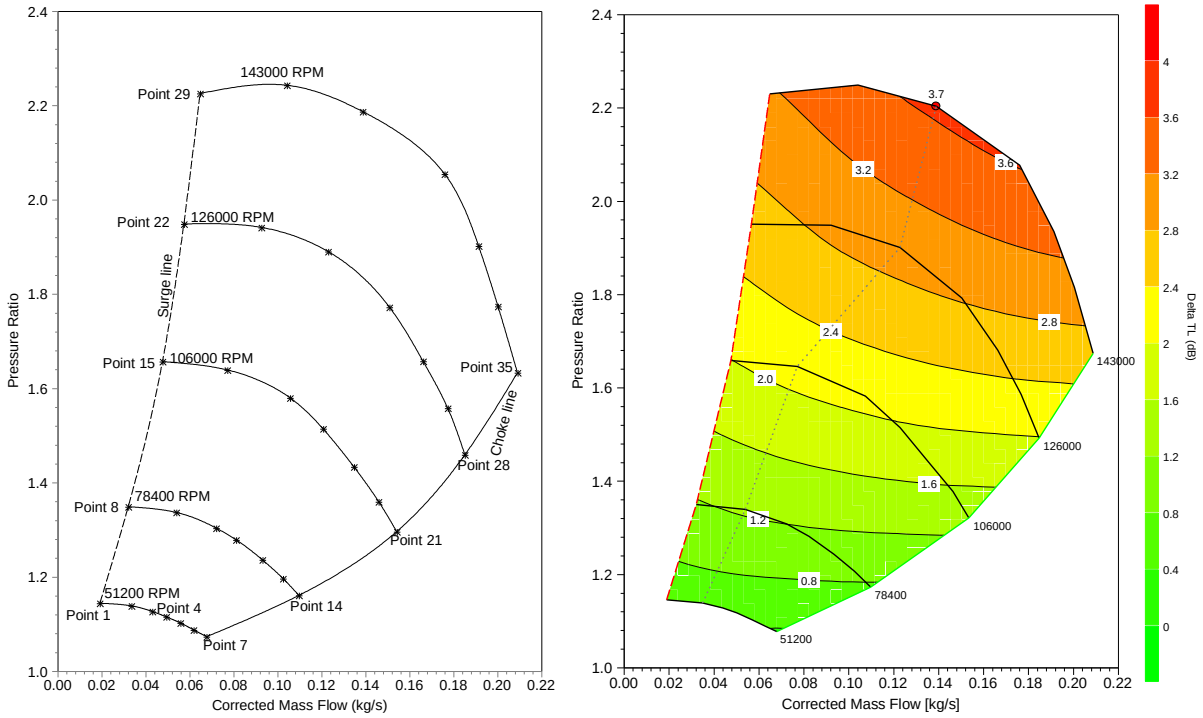

(a) Raw compressor Map (b) TL difference map

Fig. 12: Compressor map

The resulting TL are plotted in Figure 13. Figures a(a) to (d) show the TL against frequency over one iso-speed line as shown in Figure 12 (a), going from the surge point to the choke point. Figure 13 (e), shows the TL obtained over the surge line of the turbocharger. It can be seen that globally the higher the rotating speed, the higher the TL. As can be seen in equation (2.3.2), this is due mainly to the high difference of conditions between the inlet and the outlet of the compressor. At relatively low rotational speeds, the conditions at the inlet and outlet are less different than at high speeds, this is traduced for example by a higher boost level on the compressor maps, which creates high differences between air densities and temperatures (thus speed of sound). Over one iso-speed line, the highest TL is found in the middle of the map. This can be seen in Figure 12 (b), where the mean difference between a corrected TL of a specific point and the reference TL (dotted line in Figure 13) of the static turbocharger is plotted.

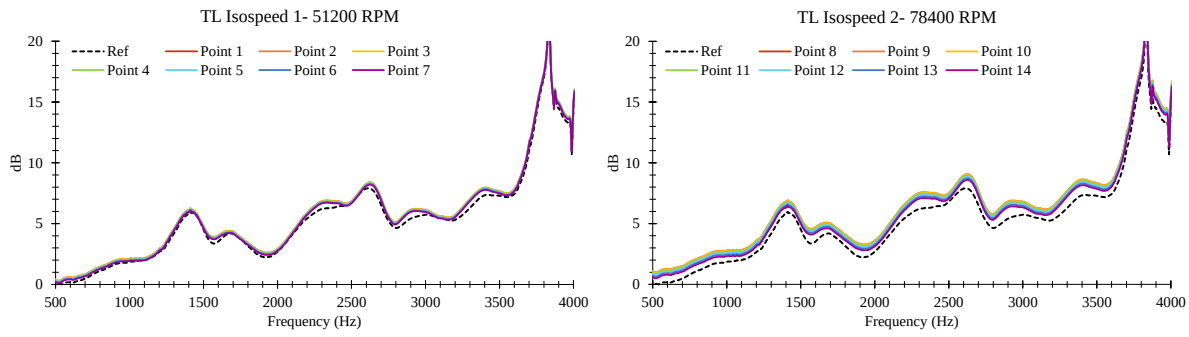

(a) (b)

Fig. 13: Transmission Loss modelled at different compressor map points

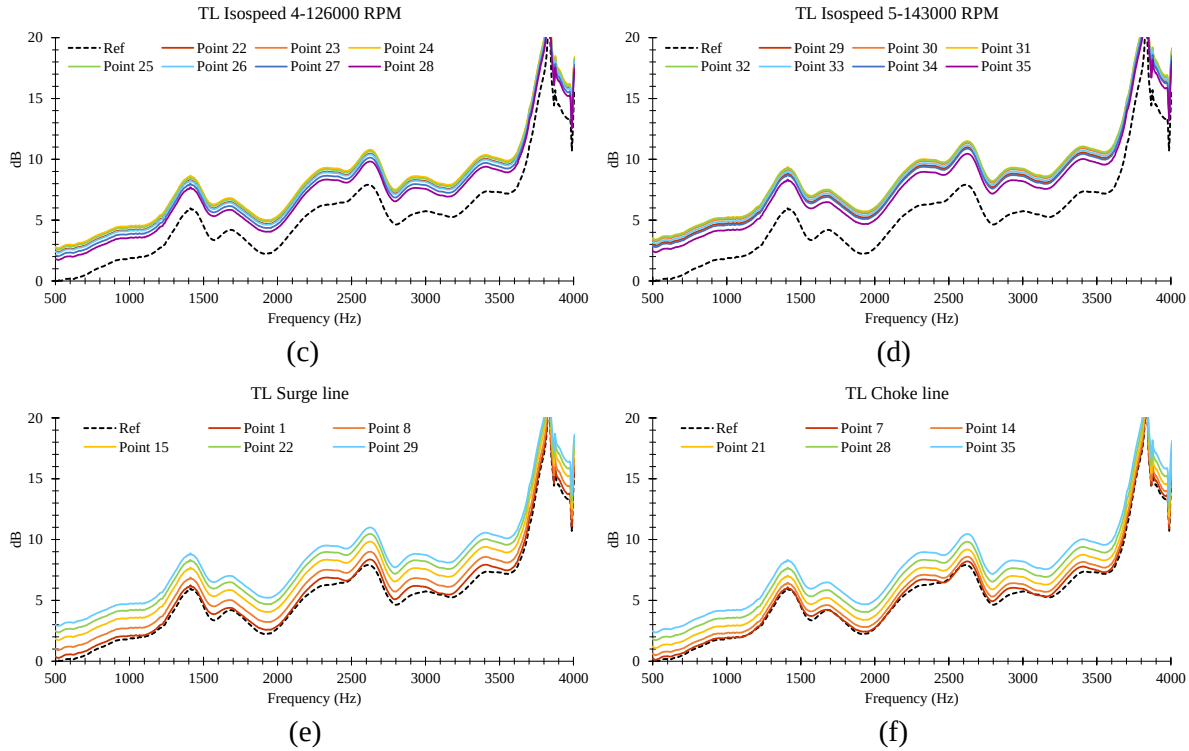

Fig. 13: Transmission Loss modelled at different compressor map points

4 Conclusions

The beamforming has been proven to be an effective way to decompose plane waves in ducts. By the way the weighting factors are calculated, the method should be sensitive only to harmonic sound, avoiding then incoherent air noise appearing in presence of air mass flow. Simulations and experimentations are being done in a simple expansion chamber geometry, in order to evaluate the influence of the mass flow noise on the beamforming measurement method. The acoustic intensity was successfully computed over all the working points of the compressor map. If a more precise analysis is needed, the frequency band of the sum level can be narrowed, and then obtain acoustic intensity corresponding to specific phenomena such as whoosh noise. The TL of a static turbocharger was successfully measured using beamforming plane wave decomposition and a scattering matrix formalism. The results were compared to 3D FE simulations and good correlation was found. Differences above 2000 Hz can be due to the estimation of the volute geometry which doesn't correspond perfectly to the real one. A simple model correcting the transmission loss over a compressor maps is proposed. The results are to be compared to experimentation, where a high level acoustic source is to be used to generate noise above the noise of the turbocharger itself, allowing then the measurement of the TL of a working turbocharger. Engine measurements have already been performed in [12], but measurements on a working vehicle are being performed so that the active acoustic characterization of a fully working turbocharger. An interesting point that has been noted is that 3D FE simulations are a technological challenge, as nowadays no commercial or open source code can deal with the rotation of the compressor wheel and the compression phenomena inside the volute. A code taking into account rotation, CFD and acoustics would be needed to confront the model. At this point, experimental data is probably more easily accessible.

References

[1] M. Abom, 'Error analysis of two-microphone measurements in ducts with flow', *The Journal of the Acoustical Society of America*, vol. 83, no. 6, p. 2429, 1988.
[2] A.J. Torregrosa, A. Broatch, R. Navarro, and J. Garcia Tiscar, 'Acoustic Characterization of Automotive Turbocompressors', presented at the THIESEL 2014 Conference on Thermo- and Fluid Dynamic Processes in Direct Injection Engines, CMT-Motores Térmicos. Universitat Politècnica de València., 2014.
[3] I. Andrés Verdu, 'Contribucion al estudio y caracterizacion de la generacion de ruido de flujo en el sistema de escape', Universidad Politécninca de Valencia, Valencia, 2003.
[4] Barry D. Van Veen and Kevin M. Buckley, 'Beamforming: A versatile approach to spatial filtering', *IEEE ASSP Magazine*, pp. 4–24, Apr. 1988.
[5] H. Bodén, 'Influence of errors on the two-microphone method for measuring acoustic properties in ducts', *The Journal of the Acoustical Society of America*, vol. 79, no. 2, p. 541, 1986.
[6] J. Bourgeois and W. Minker, *Time-domain beamforming and blind source separation: speech input in the car environment*. New York, NY: Springer, 2009.
[7] Emmet J. English, 'A measurement based study of the acoustics of pipe systems with flow', PhD Thesis, University of Southampton, 2010.
[8] Hans Rämmal and Mats Åbom, 'Experimental Determination of Sound Transmission in Turbo-Compressors', *SAE International*, 2009.
[9] Hans Rämmal, 'Studies of flow duct acoustics with applications to turbocharged engines', Royal Institute of Technology (KTH), Stockholm, Sweden, 2009.
[10] Heiki Tikkoja, Hans Rammal, Mats Åbom, and Hans Bodén, 'Test-rig for Complete Acoustic Characterization of Turbochargers', presented at the 16th AIAA/CEAS Aeroacoustics Conference, 2010.
[11] Heiki Tikkoja, Mats Åbom, and Hans Bodén, 'Investigations of Automotive Turbocharger Acoustics', *SAE Int. J. Engines*, vol. 4, no. 2, pp. 2531–2542, 2011.
[12] I. Jaimes, A. Millot, and J. Charley, 'Sound intensity measurements in turbocharger compressor ducts using multi-microphone arrays', presented at the Automotive NVH Comfort, Le Mans, 2016.
[13] K. R. Holland and P. O. A. L. Davies, 'The measurement of sound power flux in flow ducts', *Journal of Sound and Vibration*, vol. 230, no. 4, pp. 915–932, 2000.
[14] M. Åbom, 'Measurement of the scattering Matrix of acoustical two ports', *Mechanical Systems and Signal Processing*, vol. 5, no. 2, pp. 89–104, 1991.
[15] A. Mimani and M. L. Munjal, 'Acoustic Analysis of a General Network of Multi-Port Elements - An Impedance Matrix Approach', *The International Journal of Acoustics and Vibration*, vol. 17, no. 1, 2012.
[16] C. L. Morfey, 'Sound transmission and generation in ducts with flow', *Journal of Sound and Vibration*, vol. 14, no. 1, pp. 37–55, Jan. 1971.
[17] M. L. Munjal, *Acoustics of ducts and mufflers: with application to exhaust and ventilation system design*. New York: Wiley, 1987.
[18] G. Pinero, L. Vergara, J. M. Desantes, and A. Broatch, 'Estimation of velocity fluctuation in internal combustion engine exhaust systems through beamforming techniques', *Measurement science and technology*, vol. 11, no. 11, pp. 1585–1595, 2000.
[19] G. Pinero and L. Vergara, 'Separation of forward and backward acoustic waves in a car exhaust by array processing', in *ICASSP-95*, Detroit, MI, 1995, vol. 3, pp. 1920–1923.
[20] A. J. Torregrosa, A. Broatch, X. Margot, and J. García-Tíscar, 'Experimental methodology for turbocompressor in-duct noise evaluation based on beamforming wave decomposition', *Journal of Sound and Vibration*, vol. 376, pp. 60–71, Aug. 2016.
[21] *REGULATION (EC) No 715/2007 OF THE EUROPEAN PARLIAMENT AND OF THE COUNCIL of 20 June 2007 on type approval of motor vehicles with respect to emissions from light passenger and commercial vehicles (Euro 5 and Euro 6) and on access to vehicle repair and maintenance information*. 2007.
[22] *REGULATION (EU) No 540/2014 OF THE EUROPEAN PARLIAMENT AND OF THE COUNCIL of 16 April 2014 on the sound level of motor vehicles and of replacement silencing systems, and amending Directive 2007/46/EC and repealing Directive 70/157/EEC*. 2014.